Available online at www.sciencedirect.com
SCIENCE DIRECT®
ELSEVIER
European Journal of Mechanics B/Fluids 23 (2004) 29–40
EUROPEAN JOURNAL OF MECHANICS B/FLUIDS

Three-dimensionality of mode transition in vortex-induced vibrations of a circular cylinder

Franz S. Hover *, Joshua T. Davis, Michael S. Triantafyllou

Department of Ocean Engineering, Massachusetts Institute of Technology, Cambridge, MA 02139, USA

Received 31 March 2003; accepted 24 April 2003

Abstract

End lift forces and hot-wire anemometry in the wake of a flexibly-mounted rigid cylinder, undergoing vortex-induced vibrations within a uniform flow, show that the spanwise correlation undergoes a sharp reduction near conditions of maximum amplitude. Peak lift force and motion amplitudes occur on the low-velocity side of this low-correlation region; the region is bounded above by the advent of frequency lock-in. Certain aspects of this correlation loss are interpreted in the context of other free- and forced-vibration tests, and highlight the sensitivity of three-dimensional effects to the physical parameters.

Keywords: Vortex-induced vibrations; Correlation length; Anemometry

1. Introduction

Among the fundamental questions concerning vortex-induced vibrations (V.I.V.) of structures are the interdependence of incident flow conditions, structural natural frequencies and modes, near-wake flow structure, and the characteristics of the V.I.V. motions induced. As the oscillation amplitude of a forced cylinder increases from zero, so does the strength of the shed vorticity. The motion tends to organize the vortex wake, enhancing correlation of the wake structure along the span. This significant growth in correlation length occurs experimentally for vibration amplitude ratios as small as $Y/D = 0.1$ [1]; numerically predicted correlation lengths have the same trend, increasing from 3.5 to 40 diameters over the amplitude ratio range 0.05 to 0.10 [2]. The intensified and organized vortex wake also imparts greater forces on the cylinder, increasing the mean and fluctuating drag and lift magnitudes; see also the review by Bearman [3].

The phenomenon of vortex-induced vibration for compliantly supported cylinders is, however, self-limiting. Under most circumstances, even with very low structural damping, the amplitude/diameter ratio peaks at between one and two diameters because of changes in the pattern and phase of the vortical patterns that result from cylinder motion. Near these transition points, the response is quite complex; it has been described by Khalak and Williamson [4] as a competition between "2S"- and "2P"-type structures [5]. This assessment was first made based on force measurements on the cylinder; the mode types were later confirmed using digital particle image velocimetry [6]. The majority of experimental work in this sensitive regime notably focuses on a single spanwise location, through hot-wire, pressure, or image velocimetry techniques. The instability of the shear layer is an inherently three-dimensional event nonetheless for higher Reynolds numbers, and the possibility of three-dimensional effects in the flow is always present.

Reported flow measurements along the spanwise direction are decidedly few, but generally confirm the model that increasing the amplitude of motion, either through forced motion or free vibrations, increases spanwise coherence [7–12]. The present work employs a spanwise rake of anemometers to create maps of velocity correlation in the near wake, both in free-vibration

* Corresponding author.
E-mail address: hover@mit.edu (F.S. Hover).

0997-7546/$ – see front matter
doi:10.1016/j.euromechflu.2003.04.002

and nearly equivalent, monochromatic forced-vibration conditions. The effort has been motivated by evidence of three-dimensionality in the transition regime, deduced from uncorrelated end lift-force measurements [13]. This loss of correlation separates conditions of high correlation, and also steady zero-degree and 180-degree phase angles, correlating with "2S" and "2P" wake structures, respectively, but it has not been observed in some other low-mass, low-damping systems.

This issue of correlation loss, especially if structural damping is involved, is central in the prediction of V.I.V. on distributed structures, when using an integrated power balance. Lightly damped structures in fact do not require any strong correlated shedding in order to vibrate at high amplitude.

2. Apparatus and experimental setup

2.1. Virtual Cable Testing Apparatus (V.C.T.A.) and carriage

All the present experiments were performed at the Ship Model Testing Tank at the Massachusetts Institute of Technology. The Virtual Cable Testing Apparatus (V.C.T.A.) and anemometer rake are located on a computer-controlled carriage, as described in [13], and shown in Fig. 1. The experimental cylinder is mounted between two foil-shaped struts that extend above the surface of the water; below, thin circular end plates bound both ends of the test cylinder with a gap less than 0.3 cm. To measure the flow-induced drag and lift forces, three-axis piezoelectric transducers are mounted at each end. A brushless servo motor connected to a linear table actuates the struts and test cylinder in the transverse direction; the cylinder is a hollow aluminum tube two meters in length (L) with a 7.62 cm outer diameter (D). The cylinder's aspect ratio is slightly greater than 26; the blockage in the tank is approximately 4.5%. All experiments described here were conducted at $Re = 3.05 \times 10^4$.

Free vibration of the rigid aluminum cylinder is achieved through a hybrid experiment-simulation using force feedback [14]. The first step in implementing this system is the development of a mass-spring-dashpot simulation model in the form

$$m\ddot{y} + b\dot{y} + ky = F, \tag{1}$$

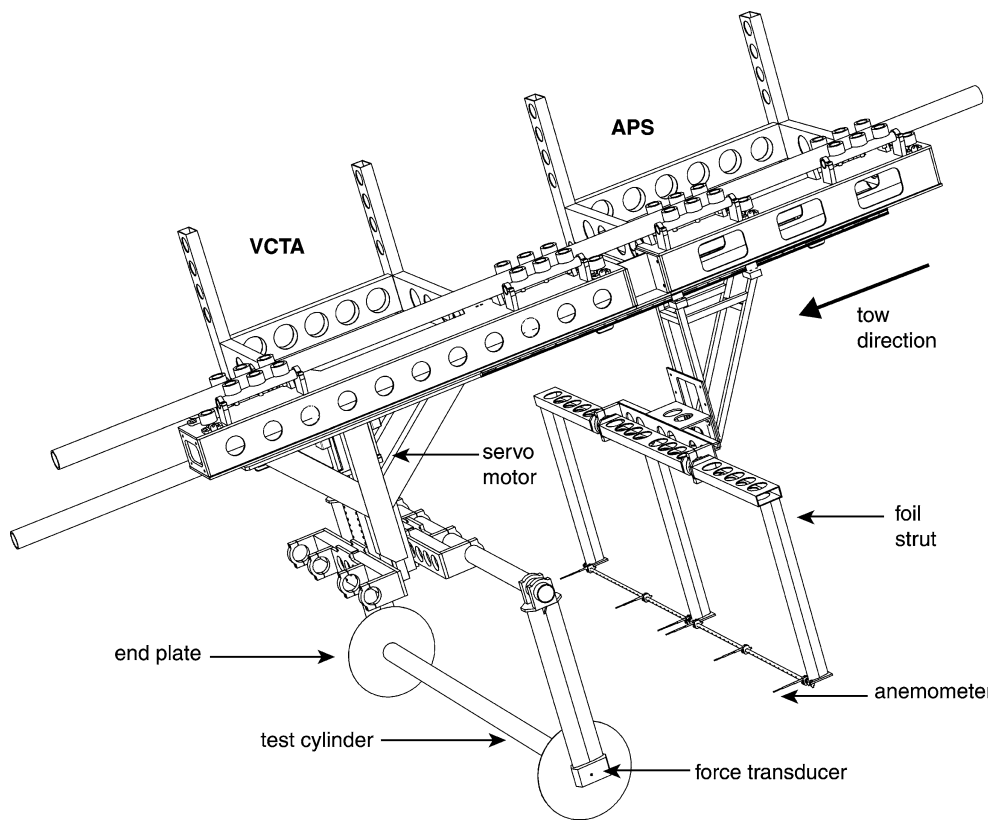

Fig. 1. The M.I.T. virtual cable testing apparatus (V.C.T.A.) and anemometer positioning system (A.P.S.).

Table 1
Spanwise location Z/D of the six anemometer probes for two configurations, and the resulting separations $\Delta Z/D$ (separations in *italics* are repeated cases)

	Arrangement α	Arrangement β
Distance from midpoint, Z/D	–4.0, –1.0, 0.0, 0.5, 2.5, 5.0	–12.5, –7.0, –5.5, 0.0, 10.0, 12.0
Separations $\Delta Z/D$	0.5, 1.0, *1.5*, *2.0*, *2.5*, 3.0, 3.5, 4.0 *4.5*, 5.0, *5.5*, 6.0, 6.5, *7.0*, 9.0, 10.0, 12.0 12.5, 15.5, 17.0, 17.5, 19.0, 22.5, 24.5	

where F is the instantaneous force imparted on the cylinder by the fluid, y is the instantaneous vertical displacement of the cylinder, and m, b, and k are the mass, damping, and stiffness of the virtual cylinder, respectively. For all free vibration experiments herein, the virtual mass ratio is $m^* = 4m\pi^{-1}\rho^{-1}D^{-2}L^{-1} = 3.0$, where ρ denotes the density of the fluid. It should be noted that this definition for mass ratio differs from some others that consider some nominal added mass to be part of the structure's mass. Although the desired virtual damping is set to zero for these experiments, the feedback loop is not ideal, and the physical damping ratio near lock-in is approximately $\zeta = 0.032$. The feedback system is implemented at 500 Hz, and in discrete-time form.

Reduced velocity, based on observed frequency ω (rad s^{-1}) is given as $V_r = 2\pi U\omega^{-1}D^{-1}$, where U is the flow speed. The nominal reduced velocity is defined similarly, but with the natural frequency (in a vacuum) of the structure, ω_n: $V_{rn} = 2\pi U\omega_n^{-1}D^{-1}$. For this work, we consider a range of $V_{rn} = 3{-}12$ for free vibrations, and then targeted values of V_r, for forced sinusoidal motions at various amplitudes.

2.2. Thermal anemometry

All experiments reported here involve the use of thermal anemometry sensors to characterize the velocity downstream of an oscillating cylinder. The anemometer probes used in the experiment are TSI hot film cylindrical, single sensor, end flow probes (model number 1210-20W). The position of an anemometer is normalized by cylinder diameter, and the streamwise component is taken positive downstream from the centerline of the cylinder; we call this streamwise position X/D. The nondimensional transverse (Y/D) and longitudinal or spanwise (Z/D) positions are defined similarly. In the case of a transversely vibrating cylinder, all anemometer positions are measured from the cylinder's rest location, where $Y/D = 0$. $\Delta Z/D$ defines the spacing of two points in the spanwise direction, and we do not distinguish positive and negative spanwise directions in this variable.

We show anemometer data primarily for the transverse locations $Y/D = [2.0, 3.0]$, at one downstream location, $X/D = 2.0$. Spanwise, the probes can be placed at 55 locations with a maximum separation of $\Delta Z/D = 24.5$ and a minimum spacing of $\Delta Z/D = 0.5$. Two specific anemometer arrangements enable a limited number of probes, six in our case, to characterize the correlation over the entire span of the cylinder; see Table 1.

2.3. Data acquisition and processing

Data are recorded at 100 Hz; after a visual inspection, the data window is selected to eliminate transients induced by the carriage starting and stopping. All the signals are low-pass filtered at 30 rad s^{-1} at the outset to eliminate noise, and lift is detrended. The following parameters are computed for each experimental run: amplitude ratio, A/D, computed from the average of the 10% highest motion amplitudes; peak frequencies ω of the lift force, the cylinder oscillation, and the wake velocities, obtained from a (non-tapered) FFT; total lift coefficient $C_l = 2F\rho^{-1}U^{-2}D^{-1}L^{-1}$, computed as the mean amplitude over repeated one-cycle windows; phase angle ϕ between the lift force and the heave motion, computed using an inner product [13]; correlation coefficient, F_c, of the two end lift forces; and for spanwise anemometry experiments, the correlation coefficient, $R(\Delta Z/D)$, taken between pairs among six anemometers.

3. Free vibration results

The summary Figs. 2 and 5 represent six sets of repeated tests, conducted for the anemometers in two different spacing arrangements (Table 1) and three transverse locations, $Y/D = [0.5, 2.0, 3.0]$. The mean value among the tests is given by the solid line; the minimum and maximum values are shown in the thin lines.

Fig. 2 illustrates the dependence of amplitude to diameter ratio and lift force characteristics on the nominal reduced velocity for all free vibration experiments. Initially, vibration amplitude increases rapidly with reduced nominal velocity. It reaches a

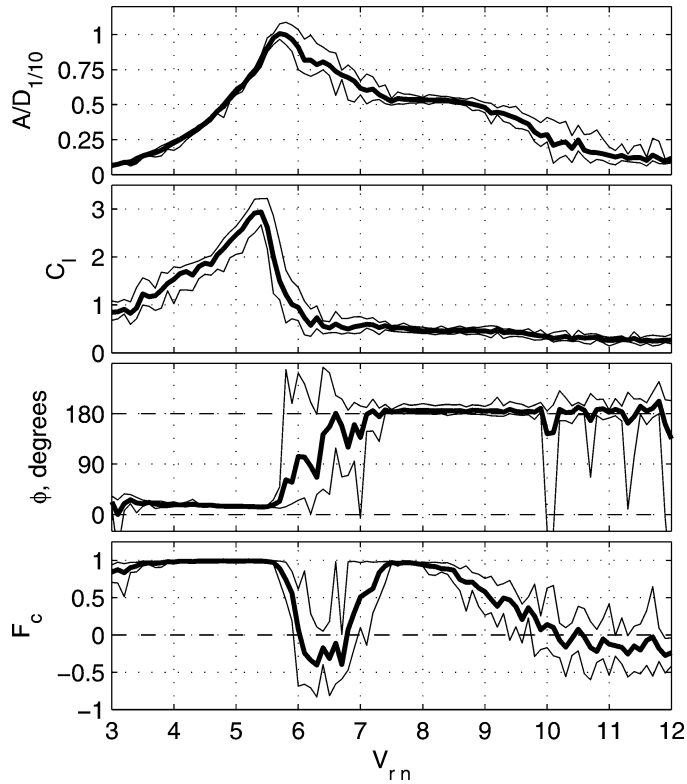

Fig. 2. Response of a freely vibrating cylinder as a function of reduced nominal velocity V_{rn}: (a) amplitude to diameter ratio A/D; (b) lift coefficient C_l; (c) phase angle ϕ (degrees) between lift force and cylinder displacement; (d) correlation coefficient of end lift forces F_c. Thin lines show the maximum and minimum values from six sets of tests; the thick line shows the mean.

maximum, narrowly exceeding unity, at $V_{rn} \approx 5.7$. At greater values of V_{rn}, the vibration amplitude ratio decreases steadily. A distinct plateau is then evident as the amplitude ratio remains nearly constant near $A/D \approx 0.55$ for $V_{rn} \approx 7.5{-}9.0$. The cylinder oscillation diminishes at the higher velocities, erratically approaching zero for the largest values of V_{rn} investigated. Fig. 2 also shows the amplitude of the lift coefficient C_l and phase ϕ of the freely-vibrating cylinder as functions of nominal reduced velocity. At low V_{rn}, the control system transfer function imposes a steady phase angle of $\phi \approx 15°$; the lift in phase with velocity ($C_{lv} = C_l \sin\phi$) takes a peak value of about 0.75 at $V_{rn} = 5.3$, and this is a condition of the structural damping absorbing a lot of power from the fluid. The peak in the total lift force slightly precedes the condition of largest A/D; lift thereafter drops quickly to 0.6, and a gradual decline with increasing V_{rn} follows. Lift in phase with acceleration $C_{la} = -C_l \cos\phi$ takes on an extreme value of about -2.8, at the same reduced velocity as the C_{lv} peak, and settles, through the phase transition region, to a value in the range 0.3–0.5. The peak value of absolute lift coefficient (2.9) is in good agreement with that reported by Khalak and Williamson [4], with indicated amplitudes of about 3.5 and 2.8 for mass ratios of 3.3 and 10.1, respectively.

A transition region in phase exists for $V_{rn} = [5.6{-}7.2]$; here, amid considerable scatter, ϕ moves to the terminal value of 180°. A close inspection of the terminal phase data shows the angle to be slightly above 180° in fact, so that the fluid is extracting a very small amount of power from the cylinder; $C_{lv} \approx -0.02$. As with the case at low V_{rn}, this imperfection is an artifact of the force feedback system.

The correlation coefficient between the lift forces measured at the two ends of the cylinder, F_c, presents a distinct "notch", indicating loss of correlation, in the same reduced velocity range over which the phase transition occurs, in accordance with [13]. Indeed, the forcing on the cylinder is well correlated, i.e., $F_c \approx 1$, for both $3 < V_{rn} < 5.6$ and $7.4 < V_{rn} < 8.5$. The lift forces are poorly correlated within the phase transition region, i.e., $5.6 < V_{rn} < 7.4$. F_c also diminishes, but only gradually, at the higher reduced velocities ($V_{rn} > 8.5$), consistent with the overall breakdown of the vortex resonance regime. The end lift force correlation is shown again, plotted on axes of amplitude and true reduced velocity V_r, in Fig. 3. The transitional loss of correlation is clearly seen at $V_r = 6.5$ and $A/D = 0.8$.

This correlation "notch" in transition is strongly influenced by the mass and damping ratios of the structure. In tests with the experimental apparatus detailed in Hover et al. [13], for example, we found that a higher value of ζ tends to improve correlation

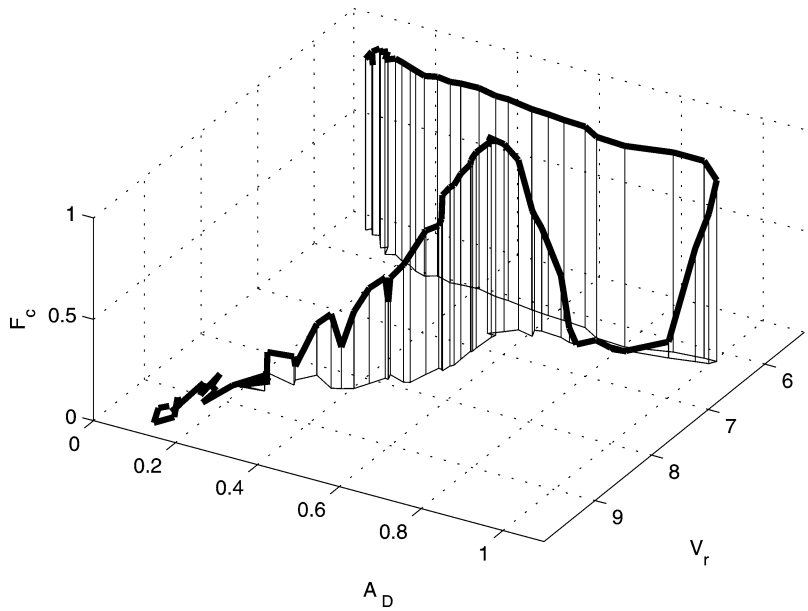

Fig. 3. End lift force correlation coefficient F_c for free-vibration tests, as a function of amplitude and observed reduced velocity V_r. F_c is constrained to be positive in this figure.

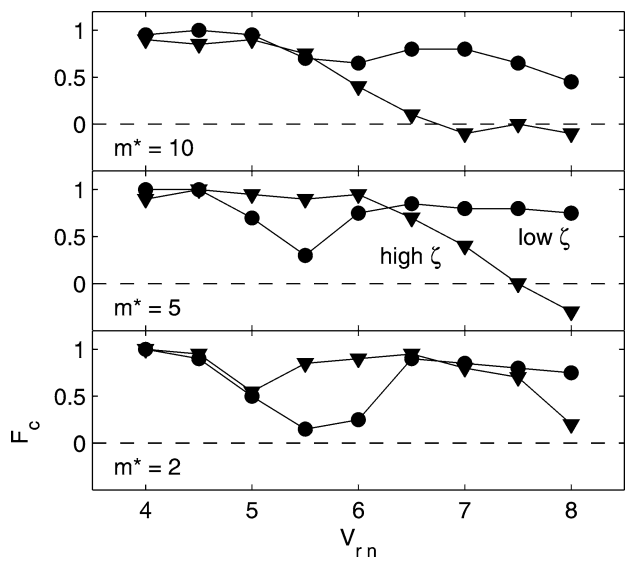

Fig. 4. Dependence of F_c on mass and damping parameters. Data are for the conditions described in [13]; low damping cases correspond with $\zeta \approx 0.01$, and high damping cases have $\zeta \approx 0.10$. Note the transitional range is $V_{rn} = 5{-}6.5$, which differs from the present experiment.

in this transitional regime; see Fig. 4. Increasing m^* improves correlation here as well, even though the vibration amplitudes at all three mass ratios and low $\zeta(\approx 0.01)$ are similar, at $0.8D$. Since the dimensional structural damping scales with both ζ and m^*, it appears that significant fluid forcing, as required to excite a damped structure, acts to correlate the local pressure field.

Fig. 5 provides the frequencies of cylinder oscillation, lift force, and downstream velocity, respectively, normalized with respect to the natural frequency of the spring-mounted cylinder, ω_n. The three frequencies are coincident for a large range of nominal reduced velocity, $V_{rn} \approx 3{-}9$. Within this range, they increase monotonically from a value of $\omega/\omega_n \approx 0.55$ at $V_{rn} = 3.0$ to a value of 1.15 for $V_{rn} = 7.1$. Above $V_{rn} = 7.1$, wake and lift frequency lock-in occurs up to $V_{rn} = 9.0$. Beyond $V_{rn} = 9.0$, first the frequency of the wake velocity, and then the frequency of the lift force begin to migrate towards the non-lock-in

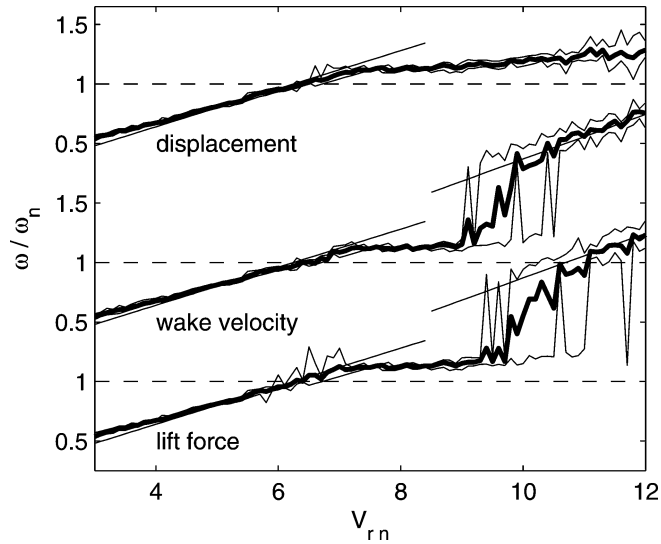

Fig. 5. Ratio of peak frequencies to natural frequency (in a vacuum) for cylinder motion, aggregate downstream velocity, and aggregate lift force, as functions of V_{rn}. Thin lines show the maximum and minimum values from six sets of tests; the thick line shows the mean.

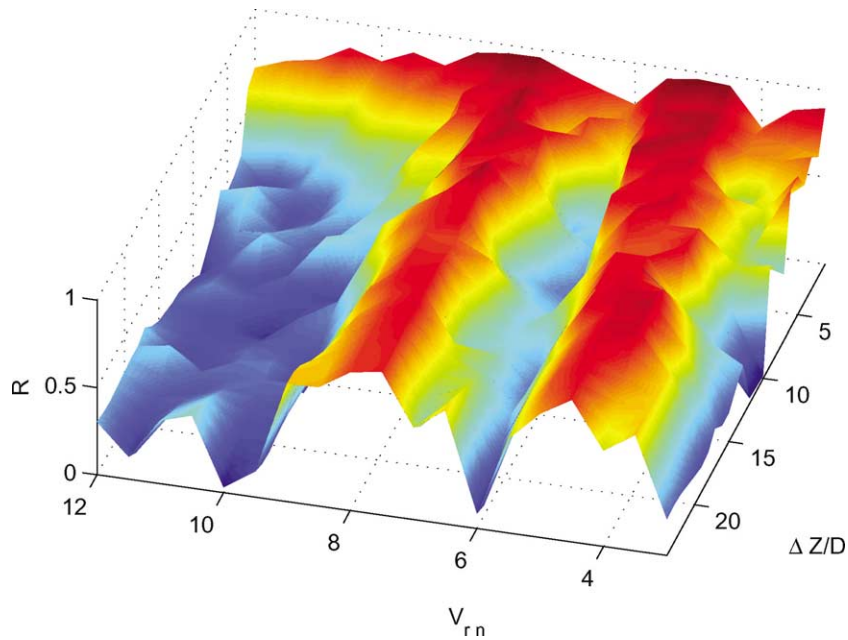

Fig. 6. Correlation coefficient of wake velocities, $R(\Delta Z/D)$, in free vibrations, as a function of spanwise separation $\Delta Z/D$.

shedding frequency. Displacement, on the other hand, remains reasonably locked-in to at least $V_{rn} = 12$. It is interesting to note that the non-dimensional shedding frequencies associated with the pre-lock-in and post-lock-in regimes are different: in the former case, the equivalent Strouhal number is 0.16, while for the latter, it is 0.187 (thin straight lines on Fig. 5). Furthermore, the actual slope of ω/ω_n taken at low V_{rn} is somewhat less than 0.16; the experimental data alone, extrapolated leftward, would have a non-zero intercept with the vertical axis.

With these V.I.V. characteristics noted, we now consider in more detail the anemometry data. The surface of wake velocity correlation coefficient, as a function of spanwise separation and V_{rn}, is given in Fig. 6; the fluid velocities measured directly downstream from the cylinder shoulder ($Y/D = 0.5$) are largely uncorrelated due to turbulence, and are not shown. Velocities measured two and three diameters above the cylinder axis are, however, significantly correlated under certain conditions. The

first correlated region, specifically $3.6 < V_{rn} < 5.6$, has values of R exceeding 0.9 at separations greater than $\Delta Z/D \approx 22$, suggesting that the wake is highly stable, solidly in the "2S" region for free vibrations [6]. The second correlation region, $7.5 < V_{rn} < 8.5$, has a similarly large contour of $R > 0.8$ at large separation distances also, indicating that the "2P" wake pattern is well organized along the span. Estimated correlation lengths, discussed below, may far exceed the length of the cylinder.

In agreement with the transitional loss of F_c between these two correlated wake regimes, we find relatively low values of velocity correlation coefficient; $R < 0.5$ for $\Delta Z/D > 5$, and $V_{rn} = 5.3 - 7.2$. This middle region is of special interest because it contains or overlaps with the most significant features in the cylinder responses.

The wake frequency lock-in, which occurs approximately in the region $V_{rn} = 7.1-9$, contains the second correlation ridge. This observation is in agreement with Ramberg and Griffin's work [9], wherein the greatest correlations are found within the lock-in region. In our case, the primary correlation loss occurs at reduced velocities below frequency lock-in ($V_{rn} = 7.2$); correlation is restored through the lock-in. On the other side, the greatest motion amplitudes ($V_{rn} = 5.7$) lie on the lower-V_{rn} end of the region of reduced wake correlation. As has been observed previously, a further defining point in the response is that of the maximal total lift coefficient, e.g., [4]. Indeed, we do find that a precipitous drop in lift (Fig. 2) also occurs coincidently with the left side of the low correlation region. Finally, we noted previously that the region of phase angle transition and the region of low correlation of the end forces (indicative of vortex pattern transformation from "2S" to "2P" modes) coincide [13]; what we find here, additionally, is that they coincide with the region of low wake correlation.

Time signals of anemometer velocity confirm the overall reduction of correlation in the regime $V_{rn} = 5.3-7.2$. In Fig. 7a, the signals are virtually identical at $V_{rn} = 5.0$, indicating that wake structures near the probe location arrive primarily in two-

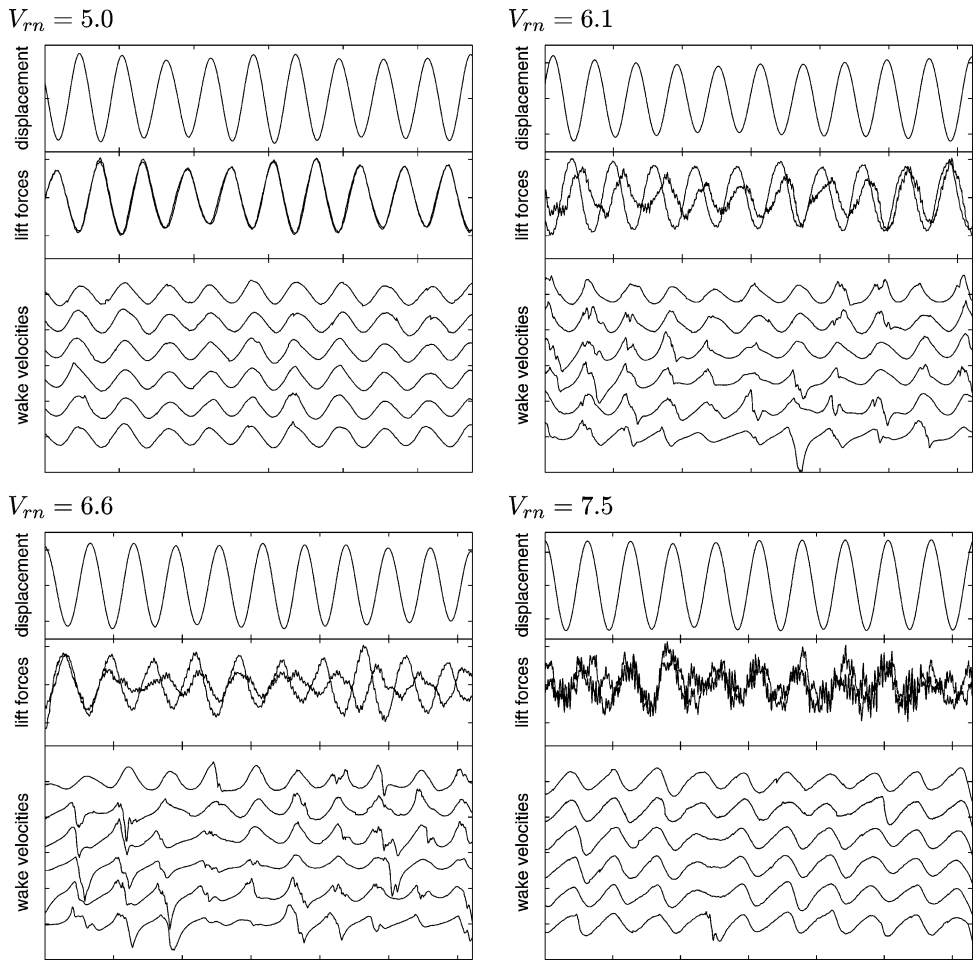

Fig. 7. Free-vibration time signals near V.I.V. transition. Vertical scaling of signals is arbitrary and is intended to show phase and correlation features.

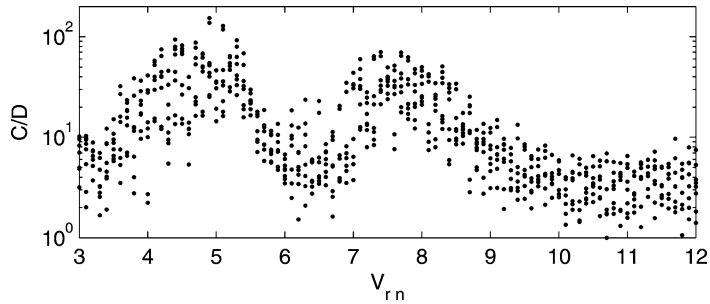

Fig. 8. Computed correlation length C/D for free vibrations.

dimensional sheets. Under this condition, the agreement of the lift forces is also quite good. At $V_{rn} = 6.1$, however, the signals become much more irregular. Velocity signals take on higher harmonics sporadically, and suffer relative phase shifts with respect to the motion, the end lift forces, and the other anemometer signals. One lift force degrades significantly, with a decreased amplitude, and a phase shift of about ninety degrees with respect to the other. At $V_{rn} = 6.6$, these properties of low correlation in velocity and force are again observed. In this particular run, the two end lift force signals are quite variable, and may alternate in size and phase through time. The anemometer signals are more corrupted also, and suffer serious sharp excursions, primarily in the negative direction (toward zero from the mean value). The terminal condition of this notch is illustrated at $V_{rn} = 7.5$. Here, although the lift signals are quite small (as shown by the reduced signal-to-noise ratio in the unfiltered data shown), their correlation is reestablished, with a phase opposite to the case below $V_{rn} = 5.7$. Anemometer signals are also brought back into close alignment under this condition, and become quite regular, except for several peaks missed by some of the probes.

The calculation of an effective correlation length C/D can be made using the simple formula

$$R(\Delta Z/D) = \exp\left[-\frac{\Delta Z/D}{C/D}\right]. \tag{2}$$

The results of this fit for the free vibrations are given in Fig. 8. The aspect ratio of the cylinder is 26, so that C/D values greater than this imply effectively correlated flow along the length. The correlation length has a clear minimum in a V_{rn} range similar to that for the end forces: $V_{rn} = 5.3{-}7.2$. Minimum correlation length in the trough is estimated to be $C/D \approx 3.5$. We found similar values at the lowest reduced velocities, i.e., $V_{rn} < 3.6$, and at the highest, i.e., $V_{rn} > 8.8$.

As a final note on the testing, we performed V.I.V. anemometry tests with both $Y/D = 2.0$ and $Y/D = 3.0$; the results were very similar, with a slight overall reduction in correlation in the latter case. This consistent degradation of the wake correlation in the phase change regime, at a location sufficiently far away from the cylinder wake, proves that the results are not merely an artifact of the anemometer probes entering the turbulent wake zone at high motion amplitudes. The breakdown of spanwise correlation for large vibrations is maintained throughout the downstream region.

4. Forced oscillations

The correlation loss which accompanies transitional V.I.V. conditions is not necessarily reflected in monochromatic forced vibrations, at equivalent frequency and amplitude [13]. This discrepancy was previously posed only in terms of the end lift force, however, and we now discuss the anemometer signals in forced vibrations chosen to cover the range of free vibrations in the previous section. A series of forced vibration tests was made, as detailed in Fig. 9. The growth region in free vibrations is covered by four separate amplitudes for a range of frequencies (A); the plateau region is covered by a different set of amplitudes and frequencies (B). At reduced velocities higher than the second range considered, we found very scattered responses in the free vibrations. As with the free vibrations, each forced vibration condition was given six separate tests: two spanwise arrangements of anemometers, and three off-axis locations.

The correlation of end forces and velocity over this range of reduced velocities and amplitudes is remarkably strong in comparison with the free vibrations. For instance, Fig. 10 shows that, in the growth region ($V_r < 5.8$), there are virtually no cases of poor end lift force correlation. Notably, at the amplitude $0.8D$, the low-V_r set of forced vibrations presents an unbroken line of correlation near unity, whereas the transitional free vibration cases in this same vicinity are poorly correlated (Fig. 3). The correlation of the forced vibrations is only reduced mildly under several conditions: at low V_r and low A/D, and at high V_r and moderate amplitude, where synchronization is known to deteriorate.

Similarly, the wake velocity correlation lengths (again for the configurations $Y/D = [2.0, 3.0]$) are shown in Fig. 10. One main feature stands out: the forced vibration cases have highest C/D in the lower V_r range, and especially for those values of

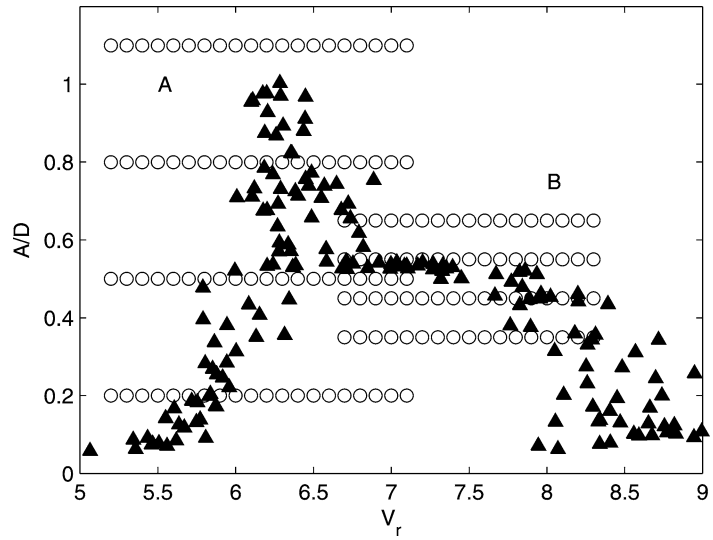

Fig. 9. Overlay of forced-vibration amplitudes and reduced velocities (circles), with (partial) free-vibration points (filled triangles). A and B denote low- and high-frequency forced vibration sets.

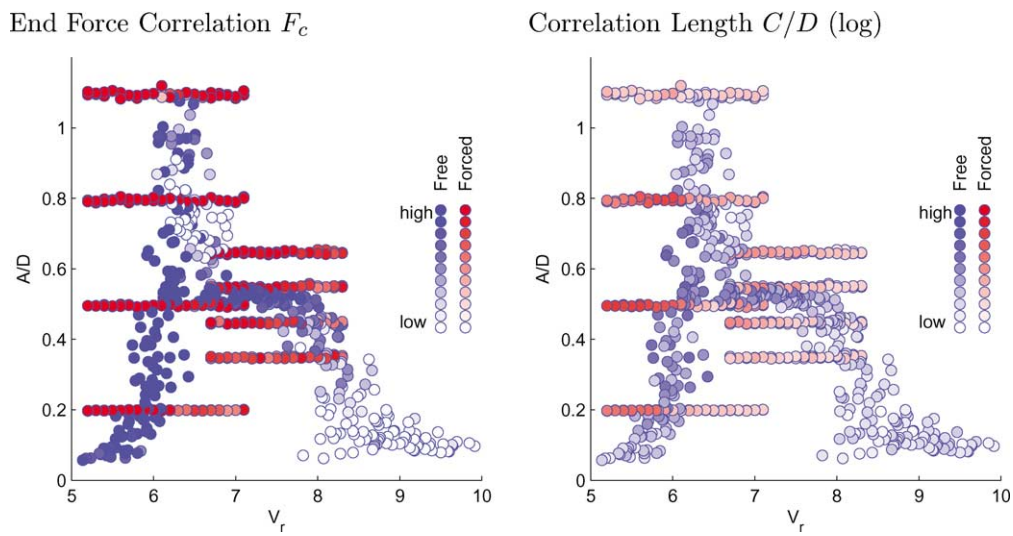

Fig. 10. Left: overlay of color-keyed F_c from free- and forced-vibration runs. White indicates a value of zero, and saturated color indicates unity. Right: overlay of color-keyed C/D. A log scale is used here; white indicates a value of unity, and saturated color indicates one thousand.

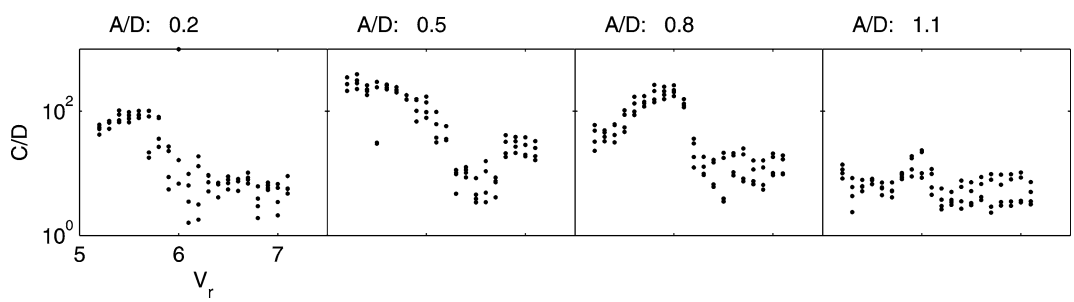

Fig. 11. Correlation length C/D for the low-frequency set of forced vibrations (A).

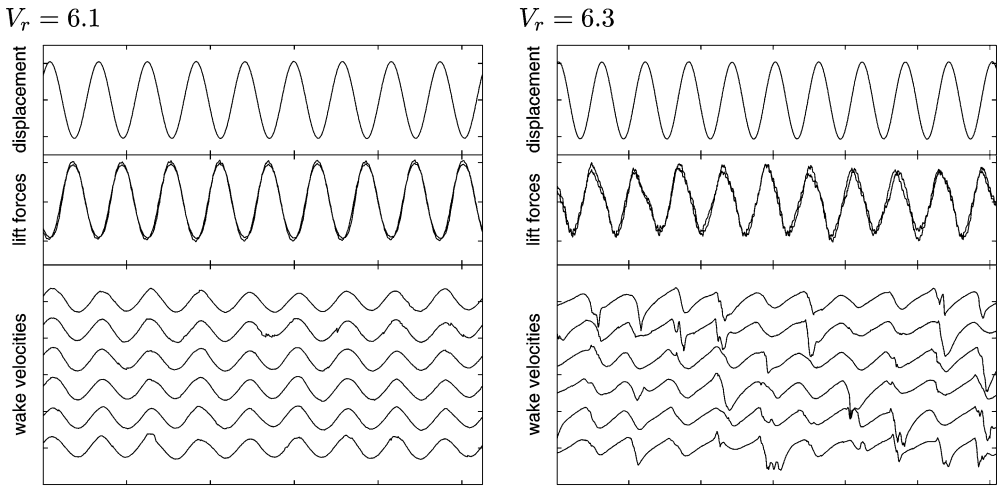

Fig. 12. Forced-vibration time signals, with $A/D = 0.8$.

V_r below those taken by the free vibration path. In fact, the loss of correlation in the forced vibrations is coincident with the path of the free vibrations in $V_r - A/D$ space. These marked changes in C/D for the forced vibrations are given also in Fig. 11. At V_r above this event, the anemometer correlations are quite similar, for the forced vibrations and for the free vibrations in transition. The A/D plateau at $V_r \approx 7-7.5$ has a slightly more organized wake for the free vibrations.

For direct comparison with Fig. 7, we show in Fig. 12 time traces for the cases $V_r = 6.1$ and $V_r = 6.3$, and $A/D = 0.8$. First, at $V_r = 6.1$, the lift forces and the anemometers are in excellent agreement, typifying the response of the free vibration in the growth regime. Increasing V_r to 6.3 leads to some slight degradation of the force signals, but with high correlation, and a significant corruption of the wake velocities, showing the same temporal and spanwise variation seen in the free vibration cases.

5. Discussion and summary

The experiments described here establish the correspondence between a fully three-dimensional wake structure and the loss in correlation between end lift forces, which we have studied previously [13]. The "2S"- and "2P"-type modes, which bracket this region of correlation loss, have been demonstrated to coexist by Techet et al. [15], using a 40:1 tapered cylinder. The vortex split described therein is, under the proper amplitude and frequency conditions, spatially stable by virtue of the taper; the two modes are phase-locked and occur at the same frequency. On an $A/D - V_r$ plot, a tapered cylinder occupies a band which shrinks to a single point as the taper approaches zero. The stability of the dislocation will hence deteriorate with reducing taper, if the band lies on a mode transition line. In this very sensitive regime, evidently the wake may: (1) switch episodically from one mode to another along the entire span (two-dimensional flow is preserved, e.g., [4]); (2) carry one, or at most a few, vortex dislocations traveling unpredictably and slowly along the cylinder span; or (3) comprise a fully three-dimensional flow, consisting of multiple irregular cells, separated by vortex dislocations. The second case is distinguished from the third by the preservation of distinct, long cells, but either case is possible if it is known only that the end forces are not well correlated. The wake velocity correlation results we have described in this paper, in contrast, clearly imply the third possibility (fully three-dimensional flow), because the second case of quasi-steady cells would bring high velocity correlation over larger spanwise length scales. Instead, the correlation is found to be close to zero within a few diameters.

This fundamental result stands in contrast with other researches, and some discussion of the possible sources of disagreement is appropriate. In our data, the low-correlation wake is primarily seen at reduced velocities beginning with the peak in lift coefficient magnitude (or, alternatively, the peak in A/D), and ending with the advent of wake frequency lock-on. Good agreement in the first of these two markers is seen in the data of Khalak and Williamson [4]: a transition area (for $m^* = 10.1$) between upper and lower branches, and centering on $V_{rn} = 5.23$, begins with the lift peak at $V_{rn} \approx 4.7$. For the same data set, however, frequency lock-in appears at very nearly the identical reduced velocity. No significant correlation loss is apparent in this reference, or in subsequent PIV tests made with the same apparatus [6].

There are several issues relevant to this type of discrepancy in V.I.V. response characteristics and the correlation. First is that of end effects. The wake behavior of low-aspect ratio cylinders can be dominated by end effects [16]; for rigid cylinder tests, some Reynolds number regimes may require an L/D ratio exceeding seventy in order to obtain any clear two-dimensional shedding at the mid-span. Great effort, through end-plates and gap control, has been made to minimize these effects in the

apparatus we use, as well as those used by others, but the precise role of the phenomenon for different arrangements has not been fully investigated under conditions of high sensitivity. Along with end effects, we may note other experimental conditions which can have an effect, such as blockage ratio, aspect ratio, and turbulence level of the incoming flow.

Additionally, and perhaps more important here, is the issue of the mass and damping parameters. The present system achieves a minimum damping ratio of 3.2% [17], so that with $m^* = 3.0$, the Skop–Griffin parameter $S_g = 2\pi^3 S^2 m^* \zeta$ is about 0.2, three times higher than that used by Khalak and Williamson. In terms of the parameter $(m^* + C_a)\zeta$ (see [6]), the present value of 0.12 puts the expected A/D peak value at only 0.6–0.9, lower than that seen in many other experiments. In short, the force-feedback approach used here cannot be considered as providing a very low damping, low mass system. For such systems, we conjecture that the loss region of correlation is inherently quite narrow, and perhaps difficult to observe in the limit of low damping. To wit, as found in [13], tests with $m^* = 3$ and $\zeta \approx 0.013$ (similar $m^*\zeta$ as in [4]) showed correlation loss in transition, but, it will be noted, over a somewhat reduced range in V_{rn} compared to the present results. Hence, although the noted discrepancy is not entirely explained by lower damping and mass, we can confirm at least a narrowing of the correlation loss region with diminishing mass and damping.

This notion of coalescence applies also to the stability of mode branches seen with low $m^*\zeta$ and other experimental systems; stable hysteretic branches would eliminate the "slow" phase transition we show in Fig. 2, which entirely contains the loss region.

At the same time, the three-dimensional nature of the near wake, at conditions of maximum amplitude under low mass-damping, has been borne out in several CFD simulations. Fig. 13 shows the lift coefficient along the span, at $Re = 1000$, $m^* = 2.0$, and $\zeta = 0.0$. The aspect ratio of the cylinder is chosen specifically to match our experiment. At the upper end of the growth region, $V_{rn} = 3.76$, the lift is very strongly correlated. As the peak condition is approached and then passed, the lift contours break down into smaller and smaller cells, which are not stationary on the span. Especially at $V_{rn} = 4.99$, we see that the correlation of lift taken at the two ends of the cylinder will be reduced by this three-dimensional flow and pressure field.

Further above the mass-damping values of the present experiment, a clear trend toward correlation is observed, as indicated previously in Fig. 4. Hence *the mass-damping emerges as a natural indicator for correlation*. High mass and damping reinforce correlation during transition, whereas moderately low values can admit a correlation loss, at least under certain conditions—the present experimental system and CFD runs.

Forced vibrations present yet an additional set of correlation data which must be assessed in consideration of the V.I.V. problem, especially if forced vibrations are to be used in a V.I.V.-prediction role. In these forced harmonic oscillations, it has been observed in general that increased amplitudes (up to a threshold point) increase correlation. In the correlation between end

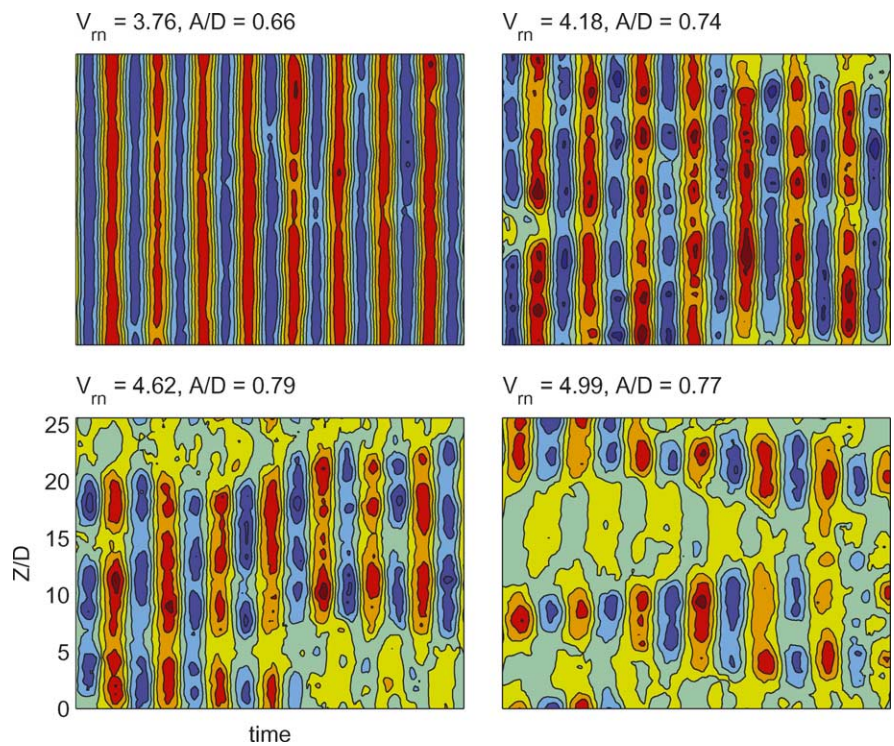

Fig. 13. Sectional lift coefficient along the span, from Brown University CFD simulation results at $Re = 1000$.

lift forces, though, the present forced vibrations yield a completely different view of transition than is seen in the free vibrations: correlation is simply never lost. The local mechanism of force production is therefore sensitive to differences in the free and forced conditions: these include additional components of the motion spectrum not included in typical forced vibrations. Since transitional V.I.V. is often—but not always—accompanied by beating (see Fig. 7 for example), this is very likely the missing component that causes loss of correlation in free vibrations.

The wake properties of free and forced vibrations are in comparatively better agreement, with the notable fact that free vibrations follow a path in the $V_r - A/D$ space that is coincident with a marked change in wake correlation for the forced vibrations, as seen in Fig. 10. The free vibration correlation is generally consistent with the forced vibration results on the high-V_r side of this change, and hence, the wake is transparent to the higher harmonics of cylinder motion, in comparison to the net lift forces. Similar wake properties are developed even when the lift forces are drastically different.

The work leaves unanswered several important questions, including the specific physical attributes which so strongly affect the flow in this sensitive regime, the mechanism by which higher damping can reinforce two-dimensional shedding, and the implications of a far wake that persists, despite extreme sensitivity to beating in the local pressure field.

Acknowledgements

This work is supported by the Office of Naval Research, under Contract N00014-95-1-0106, monitored by Dr. T.F. Swean, Jr. CFD runs were kindly performed by D. Lucor and Prof. G. Karniadakis at Brown University.

References

[1] S.-S. Chen, Flow-induced Vibration of Circular Cylindrical Structures, Hemisphere, Washington, 1987.
[2] T. Sarpkaya, Vortex-induced oscillations: A selective review, J. Appl. Mech. 46 (1979) 241–258.
[3] P.W. Bearman, Vortex shedding from oscillating bluff bodies, Ann. Rev. Fluid Mech. 16 (1984) 195–222.
[4] A. Khalak, C.H.K. Williamson, Motions, forces, and mode transitions in vortex-induced vibrations at low mass-damping, J. Fluids Struct. 13 (1999) 813–851.
[5] C.H.K. Williamson, A. Roshko, Vortex formation in the wake of an oscillating cylinder, J. Fluids Struct. 2 (1999) 355–381.
[6] R. Govardhan, C.H.K. Williamson, Modes of vortex formation and frequency response of a freely vibrating cylinder, J. Fluid Mech. 420 (2000) 85–130.
[7] H.L. Grant, The large eddies of turbulent motion, J. Fluid Mech. 4 (1958) 149–190.
[8] G.H. Toebes, The unsteady flow and wake near an oscillating cylinder, J. Basic Engrg. 91 (1969) 493–505.
[9] S.E. Ramberg, O.M. Griffin, Velocity correlation and vortex spacing in the wake of a vibrating cable, J. Fluids Engrg. 98 (1976) 10–18.
[10] S. Szepessy, On the spanwise correlation of vortex shedding from a circular cylinder at high subcritical Reynolds number, Phys. Fluids 6 (7) (1994) 2406–2416.
[11] M. Novak, H. Tanaka, Pressure correlations on a vibrating cylinder, in: K. Eaton (Ed.), Proc. 4th Int. Conf. on Wind Effects on Buildings and Structures, Cambridge Univ. Press, Heathrow, 1977, pp. 227–232.
[12] M. Hayakawa, F. Hussain, Three-dimensionality of organized structures in a plane turbulent wake, J. Fluid Mech. 206 (1989) 375–404.
[13] F.S. Hover, A.H. Techet, M.S. Triantafyllou, Forces on oscillating uniform and tapered cylinders in crossflow, J. Fluid Mech. 363 (1998) 97–114.
[14] F.S. Hover, M.S. Triantafyllou, Combined simulation with real-time forced feedback: A new tool for experimental fluid dynamics, in: T.E. Djaferis, I.C. Schick (Eds.), System Theory: Modeling, Analysis, and Control, Kluwer Academic, Boston, 1999, pp. 463–474.
[15] A.H. Techet, F.S. Hover, M.S. Triantafyllou, Vortical patterns behind tapered cylinder oscillating transversely to a uniform flow, J. Fluid Mech. 363 (1998) 79–96.
[16] C. Norberg, An experimental investigation of the flow around a circular cylinder – influence of aspect ratio, J. Fluid Mech. 258 (1994) 287–316.
[17] F.S. Hover, H. Tvedt, M.S. Triantafyllou, Vortex-induced vibrations of a cylinder with tripping wires, J. Fluid Mech. 448 (2001) 175–195.